Manuscript prepared for Atmos. Meas. Tech. Discuss.
with version 3.5 of the LaTeX class copernicus_discussions.cls.
Date: 10 October 2012

A new Method for nocturnal aerosol measurements with a lunar photometer prototype

A. Barreto[1], E. Cuevas[1], B. Damiri[2], C. Guirado[1,3,4], T. Berkoff[5], A. J. Berjón[1], Y. Hernández[1], F. Almansa[1], and M. Gil[6]

[1]Izaña Atmospheric Research Center, Meteorological State Agency of Spain (AEMET), Spain
[2]Cimel Electronique, Paris, France
[3]Institute of Environmental Assessment and Water Research, Spanish National Research Council (CSIC), Spain
[4]Atmospheric Optics Group, Valladolid University (GOA-UVA), Spain
[5]University of Maryland Baltimore County, Baltimore, Maryland, USA
[6]Instrumentation and Atmospheric Research Department, National Institute for Aerospace Technology (INTA), Spain

Correspondence to: Emilio Cuevas
(ecuevasa@aemet.es)

Abstract

This paper presents the preliminary results of nocturnal Aerosol Optical Depth (τ_a) and Angström Exponent (α) obtained from a new lunar photometer prototype, trade name Cimel CE-318U. Due to the variation of the moon's illumination inherent to the lunar cycle, the typical Langley-plot Method used in solar photometry to calibrate these instruments cannot be applied. In this paper we propose three different methods to carry out the lunar-photometer calibration. In order to validate the results we have selected three events, which encompass seven nights and ten days under different atmospheric conditions, including several saharan dust intrusions episodes. Method#1 is introduced in this work as a modification of the usual Langley Method. This technique, called Lunar-Langley Method, requires the extraterrestrial irradiances from a lunar irradiance model, providing similar accuracies on τ_a to those of AERONET ($\pm$0.01-0.02). It makes comparable daytime and nighttime measurements. Method#2 consists of transferring the current calibration from a master used by sunphotometers. Its results are again within the limit of accuracy expected for the instrument. Method#3 uses an integrating sphere and the methodology proposed by Li et al. (2008) to determine sky calibration coefficients (C_j) and the instrument's solid angle field-of-view (Ω), respectively. We observe significant τ_a differences between Method#1 and #3 (up to 0.07), which might be attributed to the errors propagation in Method#3. The good results obtained from the comparison against a second CE-318U prototype, and against daytime data from a Precision Filter Radiometer constitute a valuable assessment of CE-318U performance. Results of α and its spectral variation ($\delta\alpha$) show good agreement between daytime and night-time, being able to identify the aerosol properties associated with each event.

1 Introduction

Atmospheric aerosols are known to impact the climate evolution but they still represent one of the largest uncertainties in climate change studies (IPCC, 2007). The high uncertainty associated to the role played by aerosols in radiative forcing on a global scale makes it necessary to obtain a global ground-based aerosol climatology. In this sense, the Aerosol Robotic NETwork (AERONET) is nowadays one of the most powerful worldwide tool (Holben et al., 1998). Aerosol Optical Depth (τ_a) at a certain wavelength is the standard parameter measured by sun-photometers such as those operating in AERONET. Spectral dependence of τ_a is mainly driven by the scattering efficiency and can be expressed by means of the classical Angström's equation (Angström, 1929). In the solar spectrum, the Angström exponent (α) is a good indicator of the dominant size of the atmospheric particles. τ_a and α data obtained from AERONET stations are used to provide independent and trustable validation to satellite-based aerosols products and to regional and global aerosol/dust models. However the lack of nighttime aerosol observations introduces some uncertainties in column aerosol estimations. Nighttime τ_a is a necessary parameter to derive a continuous sequence of total column aerosol information which is of considerable importance for monitoring aerosol transport, for high latitude locations, given the extended periods of darkness during winter, to study the effect of aerosol particles on cloud lifetime and coverage during the night, and for detecting massive aerosol outbreaks at night (Zhang et al., 2008).

Ground or spaceborne lidar observations have the capability to detect atmospheric column aerosols at night. However, its spatial coverage is limited and the τ_a observations can no longer constrain the extinction solution from the backscattering observations (Zhang et al., 2008). Passive sensors for τ_a measurements at night must solve the problem of the low incoming energy from the nocturnal celestial bodies, which emit in a range of 10^{-5} - 10^{-6} the sun's energy in the case of the moon, and five orders of magnitude less for the brightest star in the sky, Sirius. On one hand, stellar photometers are proven to be more effective in determining τ_a at nighttime than lunar photometers. However, the complexity of the large-aperture instrumentation needed to capture the low-income energy from the stars limits the use of stellar photometers and their implementation in standardized regional or global networks. On the other hand, the relatively high irradiance from the moon provides the possibility of using common-aperture photometers to retrieve aerosol properties at night. Nevertheless the moon can be considered a solar diffuser with an exceptional stability, although the apparent brightness of this celestial body changes continuously with the lunar viewing geometry, such us the lunar phase or the libration angles, and due to the non-lambertian reflectance properties of its surface. As Herbet et al. (2002) suggested, the nocturnal calibration in lunar photometry is an important obstacle to overcome, because it is not stable for longer than 1 day and therefore the typical Langley procedure must be used for every nocturnal measurement. This problem was tackled by Berkoff et al. (2011) by considering a lunar irradiance model which explicitly accounts for the effects of phase, the spatial variegation of the lunar surface, the changes in the hemisphere of the moon presented to an observer (the lunar librations) and the strong backscatter enhancement at low phase angles (the so-called ”opposition effect”) (Kieffer and Stone, 2005). This empirical model, known as ROLO (RObotic Lunar observatory), was developed at the United States Geological Survey (USGS) as a NASA-funded project in support of the Earth Observing System (EOS) program. ROLO enables using the moon as a radiometric calibration source for on-orbit calibration of Earth observing satellites by means of a lunar spectral irradiance model that was developed from extensive telescopic observations acquired over more than 8 years (Kieffer and Stone, 2005). Kieffer and Stone (2005) found band-average residuals less than 1% by fitting thousands of ROLO observations at wavelengths from 350 to 2450 nm. Consequently, the model provides the exo-atmospheric lunar spectral irradiance with high precision for any given location and time within the model's valid geometric range of phase angles ±90 degrees. Berkoff et al. (2011) combined this information with nocturnal photometric measurements using a classical Cimel 318 sunphotometer to obtain atmospheric columnar multi-wavelength τ_a values. They studied this magnitude for two different atmospheric conditions near full-moon, and used a sun-photometer that was limited by a non-ideal laboratory based calibration. However, their results showed relatively low differences between observed τ_a values and those retrieved by close-in-time AERONET observations in the case of low and stable τ_a conditions. For the high and non-stable τ_a period, this study showed higher uncertainties in τ_a, especially in shorter-wavelength bands, resulting from the dark noise limit of the post-photodiode electronics. Moreover, these authors proposed the improvement of the photo detector signal-to-noise ratio in order to use this type of photometers during the bright half of lunar phase and over much wider range of wavelengths and conditions. Concerning problems derived from calibration uncertainties, they can be partially fixed with a mountain-top Langley calibration or collocating stellar reference measurements.

In this study we have used two prototypes of a new instrument developed by *Cimel Electronique* for lunar photometry, trade name CE-318U photometer, specifically designed to track the moon and to perform automatic lunar irradiance measurements. These instruments were installed at the high mountain Izaña Observatory (2400 m a.s.l.) in order to characterize their performance, to obtain absolute calibrations and to develop a reliable and trustable validation against reference instruments. We examined τ_a and α retrievals under very different nocturnal atmospheric conditions, including saharan dust intrusions with high τ_a, during a relatively long period, and compared them with daytime observations.

This paper starts with a brief description of the experimental site and its facilities (Section 2). In Section 3 the CE-318U instrument is briefly described as well as the main spectral and temporal characteristics of the lunar measurements. In Section 4 we detail the methodology to obtain τ_a and α, which requires an ad-hoc calibration procedure in case of lunar observations. Three methods have been used to assess the instrument calibration: the Lunar-Langley Method, the calibration transference from a master, and the calibration using an integrating sphere, which are presented in Section 5. The main results of this study are summarized in Section 6, where we analyze and compare lunar τ_a obtained by means the Lunar-Langley and our ROLO model implementation, showing some case analysis. We also compared τ_a and α obtained during night period with daytime τ_a and α. Finally, the main conclusions of this work are presented in Section 7.

2 SITE INFORMATION

The high mountain Izaña Observatory, managed by the Izaña Atmospheric Research Centre (IARC), from the State Meteorological Agency of Spain (AEMET) is located in Tenerife (Canary Islands, Spain; 28°18N, 16°29W, 2363 m a.s.l.). This observatory is most of the time representative of free troposphere conditions, mainly in the night period where a downward catabatic regime is well established, providing excellent conditions for accurate measurements of trace gases. A strong temperature inversion layer normally located between 800 and 1500 m a.s.l., below the Izaña level, prevents the arrival of local or regional pollution from lower levels at the Observatory. This Observatory is part of the World Meteorological Organization (WMO) Global Atmospheric Watch Programme (GAW) and part of the Network for the Detection of Atmospheric Composition Change (NDACC). Furthermore, Izaña is a suitable place for sky observations due to a high atmospheric stability, high frequency of pristine days, a low and stable total column ozone and a very dry atmosphere. Several radiometric techniques, such as FTIR (Fourier Transform Infrared spectrometry), UV (i.e. Brewer spectrophotometers), DOAS (Differential Optical Absorption Spectroscopy) and Lidar have been used for a long time.

For our purposes it is worthy to highlight that Izaña Observatory is a direct-sun calibration site of AERONET (http://aeronet.gsfc.nasa.gov) and for its associated networks PHOTONS (*PHOtometrie pour le Traitement Operationnel de Normalisation Satellitaire*; http://loaphotons.univ-lille1.fr/photons/) and RIMA (*Red Ibérica de Medida fotomtrica de Aerosoles*; http://www.rima.uva.es). In fact, PHOTONS, RIMA and IARC forms the present AERONET-Europe calibration infrastructure within the European project ACTRIS (Aerosols, Clouds, and Trace gases Research InfraStructure Network; http://www.actris.net), and Izaña Observatory is the site where master sunphotometers of AERONET-Europe are sun-calibrated. Izaña Observatory is part of the GAW Precision Filter Radiometer (PFR) network, managed by the World Radiation Center (Davos; Switzerland), whose mission is to obtain high accuracy long term τ_a and α series. Finally, Izaña Observatory hosts the reference triad of the WMO-GAW Regional Brewer Calibration Center for Europe (RBCC-E) (http://www.rbcc-e.org).

3 INSTRUMENTATION

3.1 The new Lunar Cimel CE-318U

The new lunar Cimel CE-318U photometer is, in essence, a similar instrument to the classical sunphotometer Cimel CE-318, extensively described in Holben et al. (1998), but with new improvements and features introduced to allow the retrieval of the reduced incoming energy from the moon. This new instrument performs nocturnal measurements with maximum gain and an approximate field of view of 1.29° at eight nominal wavelengths of 1640, 1020, 938, 937, 870, 675, 500 and 440 nm. 380 nm and 340 nm channels were not included due to the low incoming energy received from the moon in this spectral range. A sequence of three measurements is taken every 30 seconds at each wavelength. These triplets allow us to detect and screen clouds in the same way that they are used in sun-photometry (Smirnov et al., 2000). A new moon tracker has been built in the system. It is based in a four-quadrant detector with new electronics to amplify the signal, incorporating a new software to process data while tracking. This new tracker is also able to track the sun with a special device containing an attenuation filter to reduce the high incoming energy.

CE-318U combines the features of the standard Cimel sunphotometers with a rather good signal-to-noise ratio (better than 60 dB). We have estimated the instrument's precision by means of triplets stability calculation for both diurnal and nocturnal measurements, following Holben et al. (1998). This magnitude accounts for both electronic and instrumental errors. As in sun photometry, each triplet value is defined as the maximum minus minimum raw data divided by the mean value of the three consecutive measurements taken every 30 seconds. Results are presented in Table 1. Triplets values are wavelength dependent, and, in case of nocturnal measurements, they are also dependent on the moon's phase. They are appreciably lower for direct-sun measurements, especially in shorter wavelength channels, where the variability in triplets is the highest. This implies that daytime measurements are more stable than nocturnal ones, although the stability in daytime and near full moon observations is quite similar.

We have used two prototypes of the new CE-318U since July 2011. The most stable was considered as the master instrument, hereinafter referred to as CE-1, and the second prototype as the secondary instrument, hereinafter referred to as CE-2.

In this study we have included three different case studies. The first one involves a period of five consecutive nights in August (from 9^{th} to 14^{th}), 2011, affected by different dust instrusions. The second one is a relatively low τ_a case study during October 11^{th} and 12^{th}, 2011, while the third one is a very low and constant τ_a event during February 8^{th} to 9^{th}, 2012.

3.2 The integrating sphere for radiances calibration

A calibration system developed for the instruments performing sky radiance measurements within the AERONET-PHOTONS-RIMA networks has been implemented at the Izaña Observatory. In such systems, the light source comes from an integrating sphere providing a homogeneous visual field. The recalibration of the sphere is accomplished three times a year by comparison to the travel NASA master Cimel sunphotometer (Guirado et al., 2012). Following Walker et al. (1991), the sphere's precision is assumed $\leq 5\%$.

3.3 ROLO Model

In this paper, we have used the model presented in Kieffer and Stone (2005) to calculate the lunar irradiance (ROLO model) using our own astronomical calculations. ROLO Project was established to characterize the brightness of the moon with the aim of addressing the critical calibration problems of the Earth remote-sensing imaging sensors (Kieffer and Stone, 2005). This program was developed at the U.S. Geological Survey (USGS) Flagstaff Science Center in Arizona as a NASA-funded project. The basis of this program is the automated ground-based observations over multiple years to capture the cyclic brightness variation of the moon. The observatory was in operation for more than 8 years, observing every clear night at lunar phases within ±90°. Over 85000 lunar images were acquired in 32 wavelengths from 350 to 2450 nm. These images form the basis data for the model, as spatially integrated lunar irradiance measurements. The ROLO model uses an empirically derived analytic equation to predict the lunar disk-equivalent reflectance (A_j) in the spectral band j using only geometric variables (Kieffer and Stone, 2005),

$$ln(A_j) = \sum_{n=1}^{3} a_{i,j} g^i + \sum_{n=1}^{3} b_{n,j} \varphi^{2n-1} + c_1 \cdot \theta + c_2 \cdot \phi + c_3 \cdot \varphi \cdot \theta + c_4 \cdot \varphi \cdot \phi + d_{1,j} \cdot e^{\frac{-g}{p_1}} + d_{2,j} \cdot e^{\frac{-g}{p_2}} + \\ + d_{3,j} \cdot cos(\frac{g - p_3}{p_4}) \quad (1)$$

where g is the absolute phase angle, θ and ϕ are the selenographic latitude and longitude of the observer, respectively, and φ is the selenographic longitude of the sun.

Kieffer and Stone (2005) found band-average absolute residuals about 1% by comparison between ROLO empirical irradiances and hundreds of ROLO observations. Consequently, ROLO provides the exo-atmospheric lunar irradiance with a relatively high precision over the full range of the geometric variables and wavelengths at a specific location and time. Since our modeled irradiances were computed using a different astronomical ephemeris calculator and taking into account that ROLO provides I_0 modeled values fro 32 specific spectral responses, probably our ROLO-implemented model had a slightly lower accuracy than ROLO. In this study we have used the Alcyone ephemeris 4.3, based on the Moshier's ephemeris and the celestial mechanics equations from Meeus (1991), both adjusted to the Jet Propulsion Laboratory's DE404 results. It has an expected precision within 0.5" in moon's longitude, 0.33" in latitude and 0.36 km in distance.

3.4 Ancillary information for data validation

τ_a and α version 1.5 obtained with the Izaña AERONET master #244 (http://aeronet.gsfc.nasa.gov), near sunset and near sunrise, are used to compare with τ_a and α determined with CE-1 and CE-2 at moonrise and moonset, respectively. Following Eck et al. (1999), the expected total uncertainty in τ_a for field AERONET Cimel instruments is 0.010-0.021, and 0.002-0.009 for master instruments.

A 4-wavelength GAW Precision Filter Radiometer (PFR) developed by the World Optical Depth Research and Calibration Center (WORCC) of the PMOD World Radiation Center (http://www.pmodwrc.ch/worcc/index.html) is in operation at Izaña since July 2001. PFR near sunset and near sunrise τ_a at 412.1, 501.0, and 863.1 nm, as well as α, were used as an additional reference to validate the CE1 and CE-2 data. Low τ_a differences between PFR and AERONET Cimel, in case of instantaneous measurements, have been reported by Nyeki et al. (2012) (0.0024 measured at Davos). Mean bias differences of 0.002 and 0.003 between PFR and AERONET Cimel were recorded at Izaña during 2011 (Dr. Christoph Wehrli, personal communication).

A Micropulse Lidar (MPL), MPL-3 (SES Inc., USA) system (Spinhirne et al., 1995) has been running at Santa Cruz de Tenerife station (28.5°N, 16.2°W; 52 m a.s.l.) since January 2005. This program has been implemented for monitoring and characterization of Saharan Air Layer (SAL) North Atlantic outflow, and it is currently in operation within NASA/MPLNET (hhttp://mplnet.gsfc.nasa.gov), and is co-managed by National Institute for Aerospace Technology (INTA; Spain) and the Izaña Atmospheric Research Centre (IARC; AEMET). Micropulse Lidar (MPL) is a robust system with high-pulse frequency (2500 Hz) and low-energy (7-10 μJ, maximal) eye-safe Nd:YLF laser at 523 nm operational in full-time continuous mode (24 hours a day / 365 days a year). Lidar backscattered signal is registered in 1-minute integrated time and with a vertical resolution of 75 m. Details of the MPL and the on-site maintenance and calibration techniques are described by Campbell et al. (2002). It is used to track the SAL dust layering structure evolution from day to day, and be compared qualitatively with τ_a evolution obtained with AERONET and lunar photometers. In this study we have processed lidar data and obtained backscatter cross sections.

FLEXible backward TRAjectories (FLEXTRA) plots from the EMPA facility for Global GAW stations have been used to confirm the pathways of air masses arriving to Izaña at several levels (Stohl et al. (1995), Stohl et al. (1998)). The calculations are based on the FLEXTRA model and driven by ECMWF wind fields with a global resolution of 1° x 1°. FLEXTRA trajectory images are available at http://lagrange.empa.ch/.

4 METHODOLOGY

4.1 Aerosol Optical Depth determination. The Lunar-Langley Method

Attenuation of moon's irradiance in an atmospheric window, as occurs during daytime, can be described by the Beer-Lambert-Bouguer Law:

$$V_\lambda = V_{0,\lambda} \cdot exp(-m(\theta) \cdot \tau_\lambda) \quad (2)$$

where V_λ is the output voltage, $V_{0,\lambda}$ represents the extraterrestrial voltage, which includes all temporal variations (lunar phase as well as earth-moon and moon-sun distances), m is the relative optical mass, function of the moon's zenith angle θ, and τ_λ is the spectral optical depth. For the air-mass and the spectral optical depth calculation we have followed the specifications corresponding to AERONET version 2. Moon's zenith angle (θ) has been obtained using the ephemeris Alcyone 4.3. Taking logarithms on both sides of Eq. (2) we have,

$$ln(V_\lambda) = ln(V_{0,\lambda}) - m(\theta) \cdot \tau_\lambda \quad (3)$$

To account for the change in moon's illumination during the course of the night as well as the distance effect on lunar irradiance, we have introduced in Eq. (2) these the two contributions on the V_0 term. Thus,

$$V_{0,j} = I_{0,j} \cdot \kappa_j \quad (4)$$

where $I_{0,j}$ is the extraterrestrial irradiance in a certain channel with a central wavelength at j, and κ_j is a constant that depends on the instrument features (calibration coefficients, C_j, and the instrument solid angle field-of-view, Ω). $I_{0,j}$ is calculated using the ROLO lunar disk-equivalent reflectances in Eq. (1). It takes into account lunar phase as well as sun-moon distance. In this work, the sun-moon distance as well as the selenographic latitude and longitude of the observer and the sun are computed using the astronomical calculator previously described. Lunar reflectances are converted to modeled irradiances using the following expression,

$$I_j = \frac{A_j \cdot \Omega_M \cdot E_j}{\pi} \quad (5)$$

In this equation Ω_M is the moon's solid angle, dependent on the moon-earth distance and E_j is the solar spectral irradiance for the band j. Following Kieffer and Stone (2005), to obtain the last term the irradiance model of Wehrli (1986) has been assumed,

$$E_j = \frac{\int_{\lambda_1}^{\lambda_2} E_s(\lambda) \cdot R(\lambda) d\lambda}{\int_{\lambda_1}^{\lambda_2} R(\lambda) d\lambda} \quad (6)$$

where $E_s(\lambda)$ is the sun's spectral irradiance at 1 AU and $R(\lambda)$ is filter response function for each spectral band of CE-318U. Regarding Ω_M, it is obtained using the topocentric apparent diameter of the moon (d_{app}), function of earth-moon distance,

$$\Omega_M = \pi \cdot (sin\frac{d_{app}}{2})^2 \tag{7}$$

With all these inputs on the Eqs. (1) and (5) moon's irradiance was calculated coincidentally with each CE-318U measurement.

The calibration methodology for nocturnal photometry proposed here for nighttime measurements is called Lunar-Langley Method. It uses equations (3) and (4) and a least squares fitting to obtain the instrument's calibration constant (κ_j) as the intercept of the fitting line. In this case κ_j constants strictly accounts for the instrument's photometric responsivity and any residual systematic offset difference between ROLO predicted $I_{0,j}$ and the actual exoatmospheric irradiance. Thus, it must be ideally computed as an average of some Lunar-Langley's obtained in a mountain-top station under suitable atmospheric conditions.

As in daytime period, a good Lunar-Langley calibration requires clean, cloud-free and stable atmospheric conditions. For this reason it is commonly applied in sun-photometry over a range of air masses between 2 and 5 during sunrise or sunset. In this study we have used the Lunar-Langley methodology to obtain the calibration constants κ_j's under stable and clear atmospheric measurements, over a range of air masses between 2 and 5 (during the moonrise or the moonset).

Once κ_j's are known by means of the Lunar-Langley Method, it is possible to determine instantaneous τ_a from an individual measurement:

$$\tau_{a,j} = \frac{ln(\frac{V_j}{I_{0,j}}) - ln(\kappa_j) - m_{atm}(\theta) \cdot \tau_{atm,j}}{m_a(\theta)} \tag{8}$$

The subscript atm accounts for air mass and optical depth of each atmospheric attenuator with the exception of aerosols.

4.2 Angström's exponent (α) determination

The Angström's exponent (α) is a measure of the wavelength dependence of the τ_a (Angström, 1929). α is a qualitative indicator of aerosol particle size (Kaufman et al., 1994), as it is inversely related to the particle size (Kim et al., 2011). Thus, the combined α-τ_a information is useful to discriminate different atmospheric aerosol types.

To obtain this parameter we have retrieved τ_a within the spectral range between 870 nm and 440 nm. Taking the slope of the linear fit to the logarithm of λ_j vs. logarithm of $\tau_a(\lambda_j)$ (j=870, 675, 500 and 440 nm channels), we can obtain α using the following equation:

$$ln(\tau_a(\lambda_j)) = ln(\beta) - \alpha \cdot ln(\lambda_j) \quad (9)$$

Another important parameter is the spectral variation of α ($\delta\alpha$). It reports additional information about the aerosol size distribution, and it is expressed as,

$$\delta\alpha = \alpha(440,675) - \alpha(675,870) \quad (10)$$

Positive values of $\delta\alpha$ indicate the coexistence of two separate particle modes. Eck et al. (1999), with a case analysis in Gobi desert, and Basart et al. (2009) with a climatology from 32 AERONET stations in Northern Africa and Middle East, demonstrated that relatively small negative values of $\delta\alpha$ indicate the presence of pure desert mineral dust.

4.3 Instrument solid angle field-of-view determination

The solid angle field-of-view (solid angle FOV or Ω) of a photometer is normally provided by the manufacturer. However, in this work we have calculated it following the methodology proposed by Li et al. (2008). It computes Ω from daytime measurements using the aureole calibration coefficients (C_a) and instrument user and internal gains, instead of computing them by means of the classical laboratory method. The C_a coefficients are obtained by means of a calibration using an integrating sphere. These authors obtained from error propagation expected uncertainties between 3% and 5%. They propose the following definition for Ω:

$$\Omega = \Omega_g \cdot \frac{LG}{HG_a} = (\frac{E_0}{V_{0,s} \cdot C_a}) \cdot \frac{LG}{HG_a} \tag{11}$$

where Ω_g is the solid angle gain corrected, LG and HG_a are the direct and aureole instrument internal electronic gains, respectively, E_0 is the extraterrestrial solar irradiance, $V_{0,s}$ is the solar extraterrestrial constant and C_a are the aureole radiance calibration coefficients, obtained using the integrating-sphere calibration technique.

Results of Ω_j are shown in Table 2, showing a spectral dependence on this magnitude. This slight wavelength dependence was also found by Li et al. (2008), although they propose to average the spectral Ω_j over all wavelengths to derive a constant value.

5 CALIBRATION STRATEGY

As for sunphotometers, lunar-photometers need a calibration procedure in order to obtain τ_a and α, and to assess their reliability and intercomparability. Sunphotometer's calibration usually needs the estimation of the voltage measured by the instrument in absence of atmosphere by extrapolation of the voltage curve in Eq. (2) to zero air mass conditions. This calibration procedure is known as Langley-plot method. It uses the sun or, as in this case, the moon as a reference light source. However, this methodology must be re-formulated to account for the moon's irradiance variation inherent to the lunar cycle.

In this paper we present the calibration strategy for the lunar CE-318U instrument, which can be approached by three different methods, depending on available calibration facilities.

5.1 Method#1: Lunar-Langley Calibration

The first method implies the determination of the calibration constants κ_j by means of the Lunar-Langley Method expressed by using the Eqs. (3) and (4). This Method requires the knowledge of the moon's extraterrestrial irradiance at any time of measurement. Once raw data and I_0's are ratioed, the calibration constants κ_j can be determined as the intercept of the least squares fitting in Eq. (3).

We have performed this calibration technique for both CE-1 and CE-2 using the lunar data obtained on February 8^{th}-9^{th}, 2012. This night was selected due to the relatively low and constant τ_a conditions, especially during moonset, where τ_a at 440 nm remained stable and near 0.02. For CE-1, this calibration was applied in other two time periods to check the stability of the calibration.

5.2 Method#2: Calibration transference from a master

The previous calibration method is very accurate, if suitable atmospheric conditions exist. For this reason, it can only be applied in mountain-top sites where very low and stable τ_a exists, as well as low humidity nighttime conditions can be attained. Only a few sites can meet these requirements, so an alternative calibration method is needed. The second proposed method is that followed by classical sunphotometers by means of intercomparisons. It is based on the calibration transference from a master instrument (Holben et al. (1998), Toledano et al. (2011)), in turn calibrated at a high mountain site. This transference technique is possible taking into account the average ratio in digital counts between coincident measurements from two lunar photometers. Being ($\overline{DC_M}$) and ($\overline{DC_i}$) the average coincident raw data for the master and the instrument i to be calibrated, respectively, we can obtain the calibration constant $V_{0,i}$ using the known value $V_{0,M}$ obtained from a master, with the following expression:

$$V_{0,i} = V_{0,M} \cdot \frac{\overline{DC_i}}{\overline{DC_M}} \tag{12}$$

5.3 Method#3: Calibration using an integrating sphere

A third method to calibrate a lunar photometer is based on the use of an integrating sphere to determine the sky calibration coefficients C_j, as Berkoff et al. (2011) followed, and the laboratory procedure developed by Li et al. (2008) to calculate Ω_j. The instrument coefficient's κ_j can be determined as follows,

$$\kappa_j = \frac{1}{C_j \cdot \Omega_j} \quad (13)$$

From Eqs. (4) and (13) we can determine experimentally the calibration coefficients for our instrument (κ_j's) deriving C_j and Ω_j. Then, it could be possible to convert at any time ROLO exo-atmospheric irradiances into the instrument V_0 parameter. $V_{0,j}$ inferred using this method has an accuracy strongly limited by the uncertainties involved in the determination of C_j and Ω_j, as well as those involved in the ROLO model.

In this study, we have used an integrating sphere calibration system implemented for PHOTONS-RIMA calibration at IARC. The main features of the integrating-sphere were described in section 3.2.

6 RESULTS

6.1 Method#1

The calibration constants κ_j's were calculated using this Lunar-Langley calibration for the two CE-318U prototypes using nocturnal measurements on the moonset of February 9^{th}, 2012, for CE-1, and the moonrise for CE-2, as no data was available for CE-2 during the moonset. This was the most pristine and stable event to perform an accurate Langley calibration. The coefficients of the two instruments are shown in Table 3.

Using the calibration coefficients from this table, nocturnal τ_a for CE-1 have been calculated for August 9^{th}-10^{th}, 10^{th}-11^{th}, 11^{th}-12^{th}, 12^{th}- 13^{th} and 13^{th}-14^{th}, 2011 and for two episodes more on October 11^{th}-12^{th}, 2011, and February 8^{th}-9^{th}, 2012, with low and stable aerosol conditions. In Figs. 1, 2 and 3 the daytime and nocturnal τ_a evolution is presented for a sequence of six days and five nights of measurements in August and the nights in October and February. Lidar backscatter vertical cross-section is shown in addition to the τ_a course for each episode in order to have independent qualitative information about the vertical structure and variability of the aerosols. For a quantitative analysis of daytime and nocturnal τ_a differences, it is necessary to establish a criterion of quasi-simultaneity. In this study we have compared nocturnal and daytime data corresponding to the consecutive 1-hour time period during sunset-moonrise (SS-MR) and moonset-sunrise (MS-SR): the first hour of the moonrise against the last hour of previous daytime data during sunset, as well as the last hour of the moonset against the first hour of subsequent daytime τ_a during sunrise. These results are shown in Table 4.

6.1.1 High τ_a conditions: saharan dust events

We used the information from FLEXTRA backward trajectories in order to infer dust source regions in the high τ_a events assigned to August, 2011. They show air mass pathways over the Sahara and the Sahel in several height levels above Izaña Observatory up to 5500 m a.s.l. from August 9^{th} to 14^{th} (not shown here for the sake of brevity). These saharan dust intrusions during August 9^{th} and 10^{th} are clearly seen in Figure 1. The first event is detected by the MPL with a maximum backscatter signal between 2.3 and 4 km height from August 9^{th} to August 10^{th} midday. After this time the signal decreases sharply, with minimum values at night. During this period some high clouds are detected by MPL at a height above 8 km, and thus, τ_a can be affected. Differences during moonrise and sunset on August 9^{th} are below 0.01 (Table 4), whithin the τ_a accuracy limit established in AERONET (Holben et al., 1998). Nocturnal data was not available to perform moonset and sunrise comparison on August 10^{th}. In the same day, these differences reached 0.02 in 440 nm during the moonrise, meanwhile they were reduced to values below 0.01 in the next moonset-sunrise period, when another intrusion started on August 11^{th}. From 5 to 23 UTC, approximately, and after this period the backscatter signal decreased slowly. This change in aerosol concentration was well captured by CE-1, with a τ_a decreasing from values up to 0.20 in 440 nm during the early night to lower than 0.10 in 440 nm, and near constant values during the latest part of this night. From Table 4 we can see that sunset-moonrise and moonset-sunrise τ_a differences are similar, below 0.02 for all channels. We had a third intrusion in this period, on August 13^{th}. In this case, the aerosol layer extended up to 5 km altitude, starting at about 22 UTC. The dust layer is perfectly captured by the lidar profile and compares quite well to the aerosol optical depth curves obtained with CE-1. Nocturnal τ_a differences during the $12^{th} - 13^{th}$ August reached 0.02 for sunset-moonrise and 0.03 for moonset-sunrise in shorter wavelenghts channels. During the moonset and sunrise of August

14^{th} differences grew to 0.04, due to the sharp τ_a increase. Meanwhile, in the sunset-moonrise of August 13^{th}, just when this intrusion starts, τ_a differences are about 0.01. Although most of the differences found were higher than the AERONET accuracy limit for τ_a, they are explained by the high aerosol variability.

Additional information can be extracted from Table 4. Similar τ_a differences during two stable nights with different moon's illumination, 9-10 August (with a mean lunar illumination of 84.7%) and 11-12 October (near full moon, 99.8%), were found and thus we can assume that τ_a accuracy is not affected by a change in $\sim 15\%$ in fraction of illumination.

6.1.2 Low τ_a conditions

In order to test the performance of this new instrument over low and stable aerosol concentrations we have included two additional events. The first clean event showed a τ_a relatively constant (around 0.07 at 440 nm) test case during two consecutive days (October 11^{th} and 12^{th}, 2011), shown in Fig. 2. This figure demonstrates a good agreement between vertical aerosol backscatter evolution and τ_a, as well as between AERONET and CE-1 τ_a values. In Table 4, τ_a differences are ≤ 0.01 during both sunset-moonrise and moonset-sunrise. Although the increment in aerosol concentration during nighttime is well captured by CE-1, it can be seen from Fig. 2 a probable calibration problem affecting the 1640 nm and 1020 nm channels between moonrise and moonset. We attribute discrepancies in 1020 nm to temperature correction. However, discrepancies in 1640 nm do not seem to be related to a general problem in longer wavelenghts, but in particular uncertainties associated to astronomical parameters determination for a particular night.

The second clean event was on February 8^{th}-9^{th}, 2012 (Fig. 3). This is a very clear night (τ_a at 440 between 0.02 and 0.04) with a relatively stable aerosol concentration during the entire night, especially over the moonset period. On february 9^{th} a Lunar-Langley was performed. In this case, as expected, moonset data matches pretty well AERONET sunrise data. Differences are slightly greater during moonrise but whithin the AERONET τ_a accuracy limit.

τ_a validation has been completed with daytime τ_a from PFR for October 11^{th} and 12^{th}, 2011, and February 8^{th} and 9^{th}, 2012. We should note that PFR has only three channels centered at 863.1, 501 and 412.1 nm. Therefore, the comparison study can only be computed for the CE-1 near coincident channels. Due to the different central wavelength between the two instruments near 440 nm, we have derived the PFR τ_a at 440 nm from the measured value at 412.1 nm using the Angström expression for two wavelengths. AERONET versus PFR, as well as AERONET versus CE-1 τ_a differences are presented in Table 5. τ_a differences in quasi-simultaneous AERONET and PFR τ_a measurements are ≤ 0.013 for all channels in October, and below 0.006 in February, similar to the differences found between PFR and CE-1 measurements, with values up to 0.012.

These results confirm the optimum performance of the CE-1 under low τ_a conditions.

Regarding nocturnal τ_a from the CE-2, τ_a differences between AERONET and CE-2 are shown in Table 6. The agreement between these two references is pretty good, within the expected accuracy of ± 0.01 for longer wavelengths and ± 0.02 for shorter wavelengths. Since comparisons of both CE-1 and CE-2 show τ_a deviations within the expected limit of ± 0.01, it indicates the robustness of this calibration method.

6.2 Method#2

τ_a results using Method#2 have been evaluated for February 9^{th} and 10^{th}, 2012. This method is based on Eq. (12) for coincident measurements with a master (CE-1) and a secondary instrument (CE-2). In our case CE-2 was calibrated using the average ratio of raw data of the two instruments during a stable and clear night period. In this sense, February 9^{th}, 2012, was the best option, with a mean background τ_a (440 nm) ~ 0.02.

The τ_a scatter-plot obtained using CE-1 and CE-2 is shown in Fig. 4. The τ_a differences and corresponding root-mean-square error (RMSE) are presented in Table 7. τ_a comparison for the day after the calibration (February 10^{th}) shows a good concordance between the values obtained from the master and the secondary instrument, with averaged differences up to 0.002.

6.3 Method#3

The third method for a lunar photometer calibration involves the determination of the sky calibration coefficients (C_j) using the integrating sphere procedure described in section 3.2. The coefficients obtained for CE-1 using this Method are presented in Table 8. For comparison with Method#1, we have derived the CE-1 sky calibration coefficients (C_j") from the κ_j coefficients in Table 3 considering the solid-angle Ω_j in Table 2. These C_j" are also presented in Table 8. Comparing these coefficients we note that those centered at 500 and 440 nm present higher relative differences, with values up to 25%. Differences in the rest of channels are below 10%. Higher discrepancies in shorter wavelengths channels might be due to uncertainties in the integrating sphere calibration technique because in these channels the sphere's radiant flux is notably reduced.

The averaged differences between τ_a obtained with the calibration coefficients calculated with this method (C_j) and those determined with Method#1 (C_j") for August $9^{th} - 14^{th}$, 2011, October $11^{th} - 12^{th}$, 2011, and February 8^{th}-$9th$, 2012, are shown in Table 9. Lower discrepancies are observed in channels 1020, 675 and 870 nm. However, only differences in 1020 nm are within the limit of instrumental precision of ±0.01-0.02. Discrepancies are significantly higher for the rest of channels, up to 0.07 for 500 nm central wavelength channel.

The previous results highlight the lower accuracy showed by Method#3, below the precision required to make comparable daytime and nighttime measurements. These discrepancies might be caused by a sum of contributions: 1) the accuracy on $I_{0,j}$ due to the implementation of the ROLO model (with an expected systematic error $\varepsilon \geq$0.01); 2) the calibration errors from the integrated sphere method to obtain C_j's (ε=0.03-0.05); and 3) uncertainties associated to the determination of the solid angle Ω (ε=0.03-0.05). Since the first contribution also affects to Method#1, it is necessary to increase the precision of the integrating sphere calibration as well as in the determination of Ω to improve the results in Method #3 .

To check the error on the last contribution we have used the solid angle value provided by the manufacturer ($\Omega_{ref} = 3.4 \cdot 10^{-4}$ sr) and the coefficients C_j presented in Table 8. Ω_{ref} is the wavelength independent solid angle assumed by Berkoff et al. (2011) to obtain nocturnal τ_a

information. A new τ_a comparison between Method#1 and #3 using Ω_{ref} is presented in Table 10. It can be seen that differences obtained are notably higher than those from table 9 for 1020 and 675 nm channels, slightly higher for 870 nm, similar for 1640 nm, slightly lower for 440 nm and considerably lower for 500 nm. These differences are higher than those reported by Berkoff et al. (2011). It might indicate that the actual solid angle used by Berkoff et al. (2011) was closer to the manufacturer's reported value. These discrepancies clearly indicate that τ_a calculation is very sensitive to the methodology to estimate Ω.

6.4 Angströms exponent

Angström values have been obtained with CE-1 for the same cases analysis as for τ_a (August 11^{th}-14^{th}, 2011, October 11^{th}-12^{th}, 2011, and February 8^{th}-9^{th}, 2012).

Nocturnal α values for CE-1 are computed as the slope of the linear regression of ln(τ_a) versus ln(λ) using channels at 870, 675, 500 and 440 nm, as shown in Eq. (9). Mean daytime α sunset and sunrise values were extracted from AERONET database. Results for τ_a at 440 nm, α and $\delta\alpha$ are presented in Table 11 for the August, 2011 case study, and in Table 12 for October 11^{th} -12^{th} event. In these tables we have included the aerosol information extracted for the sunset (SS) and the moonrise (MR) as the average of the last 1-hour data measured during daytime and nighttime, respectively. Moreover, we have considered data corresponding to sunrise (SR) and moonrise (MR), as the first 1-hour data of each day and night.

α data derived in the two case studies range from 0.1 to 1.2. The prevalence of low α values indicate the presence of large particles (>1μm) during the saharan dust outbreaks. Minimum values below 0.2 are obtained for the periods August 9^{th}-10^{th} and 13^{th}-14^{th}, which coincide with two important saharan dust intrusions over Tenerife and a maximum $\tau_a > 0.4$ (August 9^{th}). According to Basart et al. (2009), $\alpha = 0.6$ represents an appropriate threshold value of dust laden air masses influenced by other aerosols, while $\alpha \leq 0.3$ indicates the presence of pure desert dust. On the other hand, $\alpha > 0.7$ are found in those days with relatively low dust concentrations ($\tau_a < 0.10$) during the October case study, suggesting the presence of other aerosols. A good concordance between daytime and nocturnal α values is found.

Finally, regarding the averages of the spectral variation of alpha ($\delta\alpha$) presented in Tables

11 and 12, we have obtained near zero or slightly negative $\delta\alpha$ values between -0.01 and 0.01 during the important dust intrusions starting on August 11^{th} and August 14^{th}. These results are consistent with the experimental values between -0.3 and 0.1 obtained by Basart et al. (2009) in case of coarse mode saharan aerosols. A stable period of $\delta\alpha$ between 0.2 and 0.3 was observed from moonset August 11^{th} to moonrise August 12^{th}, and from moonset August 12^{th} to moonrise August 13^{th}. For October event, higher $\delta\alpha$ values are retrieved, between 0.3 and 0.4. The low τ_a during this period (around 0.07 at 440 nm) and the positive values of $\delta\alpha$ indicate the existence of a bimodal-size distribution (O'neill et al. (2001), Eck et al. (1999)). These $\delta\alpha$ usually occurs when accumulation and coarse mode aerosols appear well-mixed (Basart et al., 2009) while relatively high positive values indicate the dominance of fine fraction aerosols (Eck et al., 1999).

7 SUMMARY AND CONCLUSIONS

In this paper we have described the preliminary results obtained with the new lunar photometer CE-318U, specifically designed to perform nocturnal photometric measurements. We have presented a first calibration strategy for this instrument which encompasses three different methods. Basically, this strategy requires the determination of the CE-318U calibration coefficients or their transference from a master instrument. The first Method consists of the adaptation of the usual Langley-plot method to nocturnal measurements. It introduces significant modifications to the current methodology, incorporating a lunar irradiance model (ROLO) to determine the instrument calibration coefficients. This strategy has been tested and validated using two CE-318U prototypes (CE-1 and CE-2), reporting discrepancies within the limit of τ_a accuracy of the instrument ($\pm$0.01-0.02). For CE-1, this calibration was applied in other time periods, demonstrating the stability of the calibration. Moreover, nocturnal and daytime τ_a comparison using AERONET and PFR under low and stable τ_a conditions on October 12^{th}, 2011, showed similar differences between AERONET/PFR, AERONET/CE-1 and PFR/CE-1, within the AERONET τ_a accuracy. This comparison, against two independent reference instruments constitutes a valuable assessment of CE-318U performance.

Method#2 consists of transferring the calibration coefficients from a master. Results showed very close τ_a between the two lunar photometers, with differences below 0.004.

Method#3 is based on obtaining the sky calibration coefficients (C_j's) using an integrating-sphere and then retrieving the calibration coefficients κ_j's once the solid angle Ω is calculated. The comparison between τ_a obtained using Method#3 and the Method#1 shows significant τ_a differences of 0.07 and 0.05 for 500 and 1064 nm channels, respectively. For the rest of channels differences are lower, below 0.05, but higher than the limit of instrumental precision expected for this instrument (±0.01-0.02). Such high discrepancies might be caused by the sum of errors in τ_a determination process using Method#3: 1) moon irradiances from ROLO model; 2) integrated sphere method to derive C_j's; and 3) the methodology to calculate Ω. Our study highlights the importance of accounting for a high-performance integrating sphere and an accurate determination of Ω to assure a good calibration following Method#3.

Finally, the comparison between daytime and nocturnal α showed a good agreement between daytime and night-time data. $\delta\alpha$ results are also in agreement with the expected values for different atmospheric conditions presented each night according to reference values reported in the literature.

The consistency of these results points to the capabilities of this new photometer to obtain aerosol properties at night. Since column aerosol optical properties are limited to the light period, this information becomes an important limitation in polar regions. In addition, monitoring the diurnal variation of aerosols is important in many sites associated to sea-land breezes, mountain-valley regime or the diurnal variations of the boundary layer height. It is also important for detecting the sharp changes that dust intrusions may experience in term of hours. Some sites with particular climatology present frequent clouds in the morning, while clear skies occurs during the night, resulting in important observation periods reduction with classical sun-photometers. Nowadays, lidar techniques, as those used in MPLNET, operate in full-time continuous mode (24 hours a day / 365 days a year) to detect qualitatively the atmospheric aerosol content and its vertical distribution. However, it is necessary to improve the lidar extinction-to-backscatter ratio using additional τ_a information provided by lunar-photometers during night-time. τ_a and α determination during the night can be used for long-term and near real time aerosol/dust models validation, as well as for new satellite-borne sensors verification. For example, the EUMETSAT Infrared Atmospheric Sounding Interferometer (IASI) sensor provides τ_a during the night (Klüser et al., 2012). So, validation of both model and satellite τ_a could be expanded to night periods. Concerning operational aerosol observations, the last eruption of the volcano Eyjafjöll, in spring 2010, highlighted the weakness of the current monitoring of this type of aerosols and the importance of having a continuous observation system to support the aircraft navigation. The joint observations of lidar/ceilometers and lunar photometers at night could help to fill monitoring gaps existing today.

To conclude, CE-318U lunar photometers in operational networks could be used as complementary instruments to expand the column aerosol observation periods and to enhance the operational capability in the Aerosol Robotic Network (AERONET). However, the complexities inherent to the lunar irradiance pattern, make lunar photometry a difficult task compared to sun-photometry. Thus, despite the good results reported in this paper, it is necessary to design a more refined calibration procedure. Further developments should be oriented to develop a photometer capable of taking measurement during both daytime and nighttime. Concerning calibration, efforts should be paid to transfer direct-sun Langley calibration to moon observations.

Nevertheless, at the present state, lunar photometry is an attractive option to complete aerosol databases.

Acknowledgements. The authors wish to thank Cimel for providing the two prototypes used in this study as well as all the technical support. In addition, we wish to express special thanks to Dr. Stone, at the United States Geological Service (USGS) for helping to implement the ROLO model and provide wise counsel to this paper. The Aeronet sunphotometer at Izaña has been calibrated within AERONET-EUROPE TNA supported by the European Community - Research Infrastructure Action under the FP7 "Capacities" specific programme for Integrating Activities, ACTRIS Grant Agreement no. 262254. The GAW-PFR network for AOD at GAW Global observatories has been implemented by the World Optical Depth Research and Calibration Center (WORCC). We want to thank Dr. Wehrli for supporting quality control and quality assurance of GAW-PFR data and for personal communications in this paper. Finally, the authors would like to express their thanks to the security staff at Izaña Observatory for kindly supporting the night operation of the lunar instruments. The integrating sphere was provided by the Infrastructure project entitled RIMA: Instrumental para infraestructura de calibracin fotométrica (RIMA-LC), Ref. UNVA05-23-038 from the Atmospheric Optics Group (GOA) at the University of Valladolid.

References

Angström, A. K.: On the atmospheric transmission of sun radiation and on the dust in the air, Geogr. ANN.,12, 130159, 1929.

Basart, S., Pérez, C., Cuevas, E., Baldasano, J.M., and Gobbi, G.P.: Mineral dust characterization for North of Africa, Northeastern Atlantic, Mediterranean Basin and Middle East from direct-sun AERONET observations, Atmos. Chem. Phys., 9, 82658282, doi:10.5194/acp-9-8265-2009, 2009.

Berkoff, T. A., Sorokin, M., Stone, T., Eck, T. F., Hoff, R., Welton, E., and Holben, B.: Nocturnal aerosol optical depth measurements with a small-aperture automated photometer using the moon as a light source, J. Atmos. Ocean. Tech., doi: 10.1175/JTECH-D-10-05036.1, 2011

Campbell, J.R., Hlavka, D.L., Welton, E.J., Flynn, C.J., Turner, D.D., Spinhirne, J.D., Scott, V.S., and Hwang, I.H.: Full-time, Eye-Safe Cloud and Aerosol Lidar Observation at Atmospheric Radiation Measurement Program Sites: Instrument and Data Processing, J. Atmos. Oceanic Technol., 19, 431-442, 2002.

Eck, T. F., Holben, B. N., Reid, J. S., Dubovik, O., Smirnov, A., O'neill, N. T., Slutsker, I., and Kinne, S.: Wavelength dependence of the optical depth of biomass burning, urban, and desert dust aerosols, J. Geophys. Res., 104 (D24), 31333-31349, 1999.

Guirado C., Ramos, R., de Frutos, Á., Berjón, A., Redondas, A., López, C., Cachorro, V., Cuevas, E., González, R., González, S., and Hernández, M.: Optical calibration facility at the Izaña Atmospheric Research Center, Opt. Pura Apl., 45 (1), 57-62, 2012.

Herber, A., Thomason, L. W., Gernandt, H., Leiterer, U., Nagel, D., Schulz, K., Kaptur, J., Albrecht, T., and Notholt, J.: Continuous day and night aerosol optical depth observations in the Artic between 1991 and 1999, J. Geophys. Res., 107 (D10), 4097, 13 PP., doi:10.1029/2001JD000536, 2002.

Holben, B. N., Eck, T. F., Slutsker, I., Tanr, D., Buis, J. P., Setzer, A., Vermote, E., Reagan, J. A., Kaufman, Y. J., Nakajima, T., Lavenu, F., Jankowiak, I. And Smirnov A.: AERONET- A federated instrument network and data archive for aerosol characterization, Rem. Sens. Environ., 66, 1-16, 1998.

IPCC, Intergovernmental Panel on Climate Change: Climate change 2007: The physical Science Basis, Cambridge University Press, U.K., 2007.

Kaufman, Y. J.: Aerosol optical thickness and atmospheric path radiance, J. Geophys. Res., 98 (D2), 26772692, 1993.

Kaufman Y. J., Gitelson, A., Karnieli, A., Ganor, E., and Fraser, R. S.: Size distribution and phase function of aerosol particles retrieved from sky brightness measurements, J. Geophy. Res.- Atmos., 99, 10331-10356, 1994.

Kieffer, H. H., and Stone, T. C.: The spectral irradiance of the moon, The Astronomical Journal, 129, 2887-2901, 2005.

Kim, D., Chin, M., Yu, H., Eck, T. F., Sinyuk, A., Smirnov, A., and Holben, B. N.: Dust optical properties over North Africa and Arabian Peninsula derived from the AERONET dataset, Atmos. Chem. Phys., 11, 10733-10741, 2011.

Klüser, L., Kleiber, P., Holzer-Popp, T., and Grassian, V. H.: Desert dust observation from space Application of measured mineral component infrared extinction spectra, Atmos. Environ., 54, 419427, 2012.

Li, Z., Blarel, L., Podvin, T., Goloub, P., Buis, J. P., and Morel, J. P.: Transferring the calibration of direct solar irradiance to diffuse-sky radiance measurements for Cimel sun-sky radiometers, Appl. Opt., 47 (10), 1368-1377, 2008.

Meeus, J.: Astronomical Algorithms, Willmann-Bell Inc., 1st edition, Richmond, Virginia, USA, 1991.

Nyeki, S., Halios, C. H., Baum, W., Eleftheriadis, K., Flentje, H., Gröbner, J., Vuilleumier, L., and Wehrli, C.: Ground-based aerosol optical depth trends at three high-altitude sites in Switzerland and southern Germany from 1995 to 2010, J. Geophys. Res., 117 (D18202), doi: 10.1029/2012JD017493, 2012.

O'neill, N. T., Dubovik, O., and Eck, T. F.: A modified Angstrom coefficient for the characterization of sub-micron aerosols, App. Opt., 40 (14), 2368-2375, 2001.

Smirnov, A., Holben, B. N., Eck, T. F., Dubovick, O., and Slutsker, I.: Cloud screening and quality control algorithms for the AERONET database, Remote Sens. Environ., 73, 337-349, 2000.

Spinhirne, J.D., Rall, J. A. R., and Scott, V. S.: Compact Eye Safe Lidar Systems, Rev. Laser Eng., 23, 112-118, 1995.

Stohl, A., Wotawa, G., Seibert, P. and Kromp-Kolb, H.: Interpolation errors in wind fields as a function of spatial and temporal resolution and their impact on different types of kinematic trajectories. J. Appl. Meteor. 34, 2149-2165, 1995.

Stohl, A., and Seibert, P.: Accuracy of trajectories as determined from the conservation of meteorological tracers. Q. J. Roy. Met. Soc. 124, 1465-1484, 1998.

Toledano, C., Cachorro, V. E., Berjón, A., de Frutos, A. M., Fuertes, D., González, R., Torres, B., Rodrigo, R., Bennouna, Y., Martín, L., and Guirado, C.: RIMA-AERONET network: long-term monitoring of aerosol properties, Opt. Pura Apl., 44 (4), 629-633, 2011.

Walker, J. H., Cromer, C. L., and McLean, J. T.: Calibration of passive remote observing optical and microwave instrumentation, in: Proc. SPIE - The International Soc. of Optical Engineering, Orlando, FL, USA, 3-5 April 1991, Vol. 1493, pp. 224230, 1991.

Wehrli, C.: Spectral Solar Irradiance Data, WMO ITD 149; Geneva: WMO, 1986.

Zhang, J., Reid, J. S., Miller, S. D., and Turk, F. J.: Strategy for studying nocturnal aerosol optical depth using artificial lights, Int. J. Rem. Sens., 29 (16), 4599-4613, 2008.

Table 1. CE-318U triplets in % obtained for two nights with different moon's fraction of illumination (FI) and for daytime measurements.

		Channels (nm)					
	Type of measurements	1020	1640	870	675	440	500
13/12/2011	Nocturnal (FI=87%)	0.36	0.18	0.23	0.26	0.61	0.52
9/02/2012	Nocturnal (FI=93%)	0.28	0.13	0.18	0.19	0.30	0.25
22/12/2011	Daytime	0.09	0.11	0.09	0.13	0.15	0.22

Table 2. CE-1 solid angle (in steradians) determined with daytime measurements.

Channel (nm)	1020	1640	870	675	500	440
Ω_j	$3.92{\cdot}10^{-4}$	$3.95{\cdot}10^{-4}$	$3.93{\cdot}10^{-4}$	$3.88{\cdot}10^{-4}$	$3.82{\cdot}10^{-4}$	$3.78{\cdot}10^{-4}$

Table 3. κ_j calibration constants extracted for each channel (in nm) for CE-1 and κ' coefficients for CE-2, both obtained on February 9^{th}, 2012 ($W^{-1}m^2nmDC$).

Channel (nm)		1020	1640	870	675	500	440
CE-1 κ_j	mean	$2.15{\cdot}10^9$	$1.28{\cdot}10^{10}$	$3.02{\cdot}10^9$	$2.29{\cdot}10^9$	$1.74{\cdot}10^9$	$1.41{\cdot}10^9$
CE-2 κ_j'	mean	$2.01{\cdot}10^9$	$1.15{\cdot}10^{10}$	$2.74{\cdot}10^9$	$2.10{\cdot}10^9$	$1.64{\cdot}10^9$	$1.33{\cdot}10^9$

Table 4. τ_a averaged differences between daytime AERONET and CE-1 data during sunset-moonrise (SS-MR, as the last 1 hour of daytime AERONET data versus the first 1 hour of nocturnal CE-1 data) and moonset-sunrise (MS-SR, as the first 1 hour of daytime AERONET data versus the last 1 hour of nocturnal CE-1 data).

	Channel (nm)	1020	1640	870	675	500	440
Aug. $9^{th}-10^{th}$, 2011	SS-MR	0.001	0.005	-0.003	0.011	-0.002	-0.006
	MS-SR	– – –	– – –	– – –	– – –	– – –	– – –
Aug. $10^{th}-11^{th}$, 2011	SS-MR	-0.010	-0.001	-0.007	-0.008	-0.009	0.015
	MS-SR	0.015	0.008	0.005	0.006	0.004	-0.003
Aug. $11^{th}-12^{th}$, 2011	SS-MR	-0.017	-0.007	-0.015	-0.015	-0.016	-0.017
	MS-SR	-0.012	-0.010	-0.013	-0.015	-0.018	-0.023
Aug. $12^{th}-13^{th}$, 2011	SS-MR	-0.016	-0.009	-0.021	-0.021	-0.022	-0.019
	MS-SR	-0.019	-0.019	-0.023	-0.025	-0.028	-0.029
Aug. $13^{th}-14^{th}$, 2011	SS-MR	-0.014	-0.009	-0.013	-0.013	-0.014	-0.013
	MS-SR	-0.024	-0.035	-0.032	-0.032	-0.031	-0.032
Oct. $11^{th}-12^{th}$, 2011	SS-MR	0.002	0.007	0.008	0.006	0.007	0.005
	MS-SR	-0.007	-0.005	-0.003	-0.004	-0.002	-0.003
Feb. $8^{th}-9^{th}$, 2012	SS-MR	- 0.006	-0.009	-0.011	-0.014	-0.016	-0.015
	MS-SR	0.001	0.001	0.001	-0.002	-0.002	-0.003

Table 5. τ_a averaged differences on October 11^{th} to 12^{th}, 2011, and February 8^{th} to 9^{th}, 2012, between daytime PFR and nocturnal CE-1 data during sunset-moonrise (SS-MR, the last 1 hour of daytime PFR data versus the first 1 hour of nocturnal CE-1 data) and moonset-sunrise (MS-SR, as the first 1 hour of daytime PFR data versus the last 1 hour of nocturnal CE-1 data). τ_a differences between PFR and AERONET during moonrise and moonset have been included.

	PFR Channel (nm)	412.1	501	863.1
PFR/CE-1	Oct. SS-MR	0.011	0.010	0.012
	Oct. MS-SR	0.011	0.010	0.009
	Feb. SS-MR	-0.008	-0.009	-0.008
	Feb. MS-SR	0.004	0.004	0.001
PFR/AERONET	Oct. SS-MR	-0.005	-0.006	-0.004
	Oct. MS-SR	-0.012	-0.013	-0.012
	Feb. SS-MR	-0.004	-0.004	-0.001
	Feb. MS-SR	-0.005	-0.006	0.001

Table 6. τ_a averaged differences between daytime AERONET and nocturnal CE-2 data for the same time period as in Tables 4 and 5 for February $8^{th} - 9^{th}$, 2012. Moonset-sunrise data was not available.

Channel (nm)	1020	1640	870	675	500	440
SS-MR	-0.005	-0.006	-0.007	-0.010	-0.013	-0.014

Table 7. τ_a averaged differences ($\overline{d}$) and RMSE for nocturnal coincident measurements of two lunar photometers (CE-2 minus CE-1) on February 9^{th} and 10^{th}, 2012.

	Channel (nm)	1020	1640	870	675	500	440
Feb 9	$\overline{d}$	0.001	0.002	0.001	0.001	0.003	0.001
	RMSE	0.001	0.002	0.001	0.001	0.003	0.001
Feb 10	$\overline{d}$	0.001	0.001	-0.001	-0.001	-0.001	-0.002
	RMSE	0.001	0.002	0.001	0.001	0.001	0.001

Table 8. Master sky calibration coefficients C_j calculated using an integrating sphere and C_j" obtained from κ_j's and solid angles previously determined, both in $Wm^{-2}nm^{-1}DC^{-1}$. The spectral relative variation between both coefficients (Δrel in %) is included.

Channel (nm)	1020	1640	870	675	500	440
CE-1 C_j	$1.16{\cdot}10^{-6}$	$2.15{\cdot}10^{-7}$	$8.95{\cdot}10^{-7}$	$1.15{\cdot}10^{-6}$	$2.02{\cdot}10^{-6}$	$1.70{\cdot}10^{-6}$
CE-1 C_j"	$1.19{\cdot}10^{-6}$	$1.97{\cdot}10^{-7}$	$8.42{\cdot}10^{-7}$	$1.13{\cdot}10^{-6}$	$1.51{\cdot}10^{-6}$	$1.88{\cdot}10^{-6}$
Δrel	2	8	6	3	25	-10

Table 9. Averaged τ_a differences ($\bar{d}$) and RMSE for five-days nocturnal period (August $9-14^{th}$, 2011, October $11-12^{th}$, 2011, and February 9^{th}-10th, 2012) obtained with calibration Method#1 and #3 using CE-1 photometer data.

Channel (nm)	1020	1640	870	675	500	440
$\bar{d}$	-0.012	0.051	0.035	0.016	0.071	0.042
RMSE	0.013	0.053	0.037	0.017	0.074	0.044

Table 10. Averaged τ_a differences ($\bar{d}$) and RMSE for five-days nocturnal period (August $10-14^{th}$, 2011, October $11-12^{th}$, 2011, and February 8^{th}-9th, 2012) obtained with calibration Method#3 and #1 using CE-1 photometer data. Solid angle was assumed as $\Omega_{ref} = 3.4 \cdot 10^{-4}$ sr., reported by the manufacturer.

Channel (nm)	1020	1640	870	675	500	440
$\bar{d}$	0.094	0.056	0.048	0.060	-0.004	0.019
RMSE	0.095	0.057	0.050	0.062	0.004	0.020

Table 11. Averaged values of τ_a (in 440 channel), α (Angström exponent) and $\delta\alpha$ obtained in August, 2011, case study. Values are for SS (sunset), MR (moonrise), MS (moonset) and SR (sunrise).

		$\tau_{a,440}$	α	$\delta\alpha$
Aug. 9^{th}	SS	0.41	0.19	0.04
	MR	0.40	0.16	0.04
Aug. 10^{th}	MS	0.40	0.16	$---$
	SR	0.32	0.12	-0.03
	SS	0.12	0.35	0.04
	MR	0.14	0.33	0.23
Aug. 11^{th}	MS	0.18	0.29	0.14
	SR	0.17	0.25	0.01
	SS	0.19	0.25	-0.01
	MR	0.20	0.23	0.02
Aug. 12^{th}	MS	0.11	0.48	0.22
	SR	0.01	0.46	0.14
	SS	0.07	0.63	0.15
	MR	0.09	0.44	0.08
Aug. 13^{th}	MS	0.09	0.56	0.17
	SR	0.06	0.68	0.20
	SS	0.07	0.63	0.16
	MR	0.08	0.53	0.17
Aug. 14^{th}	MS	0.12	0.12	0.06
	SR	0.15	0.24	0.02
	SS	0.30	0.16	0.05

Table 12. Averaged τ_a in 440 nm, α and $\delta\alpha$ for October $11 - 12^{th}$, 2011. Values are for SS (sunset), MR (moonrise), MS (moonset) and SR (sunrise).

	October $11^{th} - 12^{th}$			
	SS	MR	MS	SR
τ_a	0.07	0.07	0.07	0.06
α	1.03	1.19	0.91	1.08
$\delta\alpha$	0.40	0.25	0.23	0.47

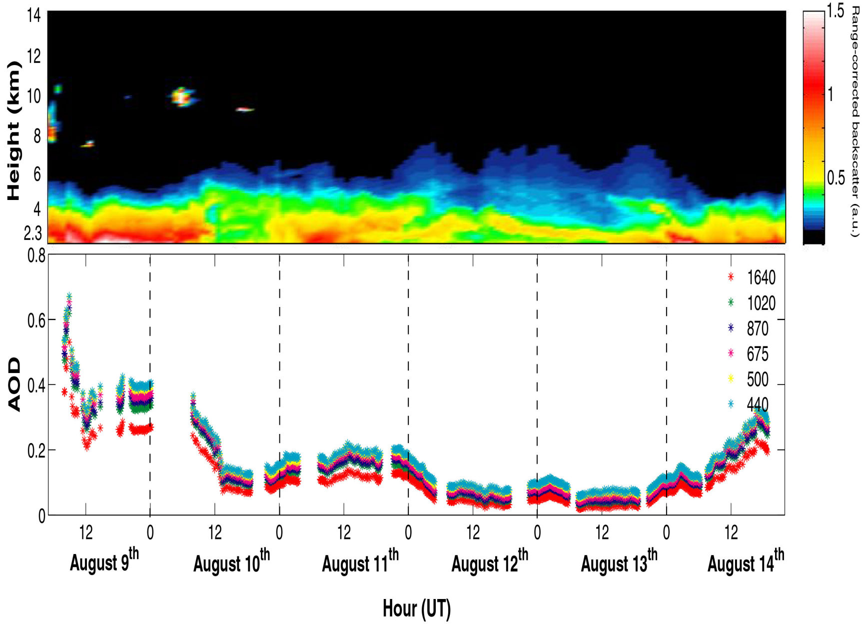

Fig. 1. τ_a evolution during six days and five nights on August, 2011, using AERONET data for daytime and lunar CE-1 data for nocturnal period. MPL corrected backscatter cross-sections obtained at Santa Cruz station from the Izaña Observatory level in upper panel.

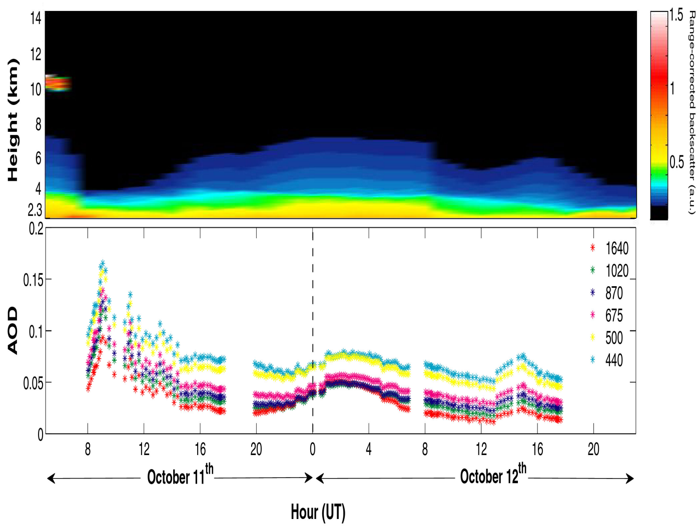

Fig. 2. CE-1 τ_a on October 11^{th} and 12^{th}, 2011, with MPL corrected backscatter cross-sections for the same period from the Izaña Observatory level (upper panel).

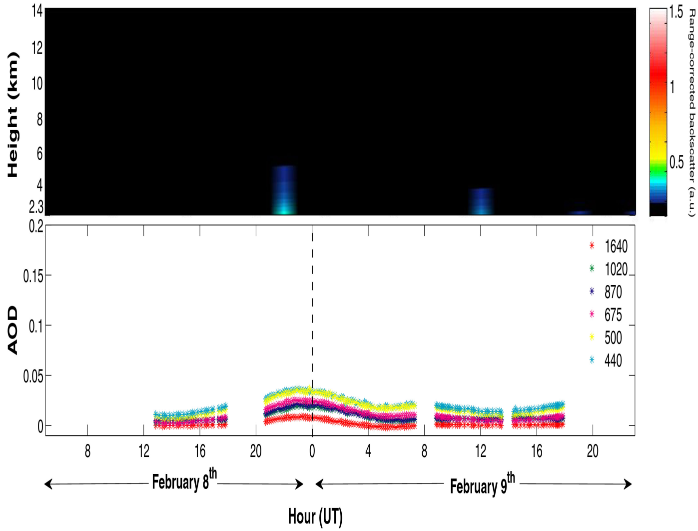

Fig. 3. CE-1 τ_a on February 8^{th} and 9^{th}, 2012, with MPL corrected backscatter cross-sections from the Izaña Observatory level.

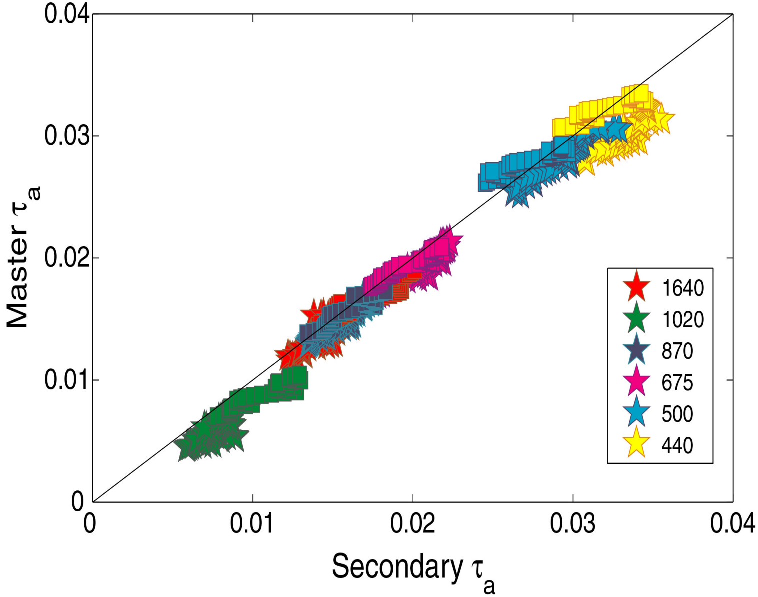

Fig. 4. τ_a scatter-plot obtained for CE-1 (master) and CE-2 (secondary) using calibration Method#2 for February 9^{th} (stars) and February 10^{th} (squares), 2012.